BULLETIN OF THE POLISH ACADEMY OF SCIENCES
TECHNICAL SCIENCES, Vol. 62, No. 4, 2014
DOI: 10.2478/bpasts-2014-0095

The vibration of prototype aircraft propeller speed reduction unit – test bench and FEM numerical simulation study

W. OSTAPSKI*, A. AROMIŃSKI, and S. DOWKONTT

Institute of Machine Design Fundamentals, Warsaw University of Technology, 84 Narbutta St., 02-524 Warszawa, Poland

Abstract. The results of torsional shaft vibration bench tests for a prototype aircraft propeller speed reduction unit are presented in this paper. The study was conducted as a function of engine speed and lubrication conditions. 3D model of the propeller speed reduction unit was developed. By using the finite element method, normal modes frequencies were defined. The simulation was conducted both unloaded and loaded under nominal power conditions.

Key words: aircraft propeller speed reduction unit, natural frequencies, FEM, bench test.

1. Introduction

A propeller speed reducing unit was design for an aircraft piston engine having an output $N = 200$ kW [1]. One condition for admission to flight tests is verification of propeller shaft's torsional vibration over the full range of working loads and rotational speeds. Many vibration sources were detected while bench testing. Internal sources of vibrations include manufacture and assembly errors, compliance and variable stiffness of elements and components, gas force pulses, characteristics of the propeller and other. External sources of vibrations include variable load operating conditions. Vibration sensors were used to record the entire spectrum of the shaft vibration measurement band. Dominant vibrations in the propeller shaft's motor-gearing system are caused by engine torque irregularities and load condition variations. Thus, identification of vibrations excited by the gearing in the spectrum of shaft vibrations is difficult. Identification of these vibrations may facilitate knowledge of vibration in the unloaded and loaded conditions, the internal excitations (assembly and operation errors), and the torsional stiffness of the propeller speed reduction unit swivel.

2. 3D model of the planetary gear unit

The propeller speed reduction unit was designed with a gear ratio of $i = 2.1$, the rotational speed of $n < 5600$ revolutions per minute, and the nominal power $N = 200$ kW [2]. Figure 1 presents the 3D model, while Fig. 2 illustrates the mesh model.

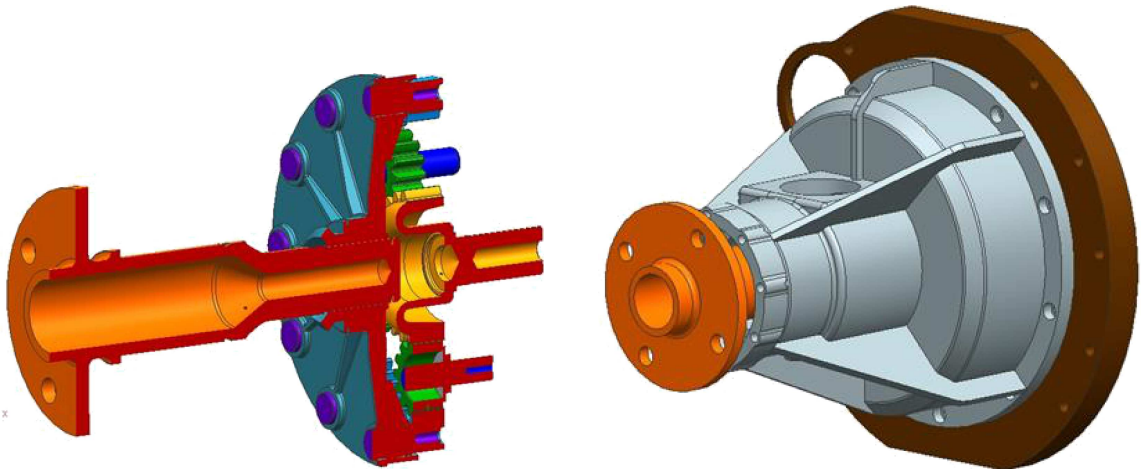

Fig. 1. 3D model of propeller speed reduction unit

*e-mail: wos@simr.pw.edu.pl

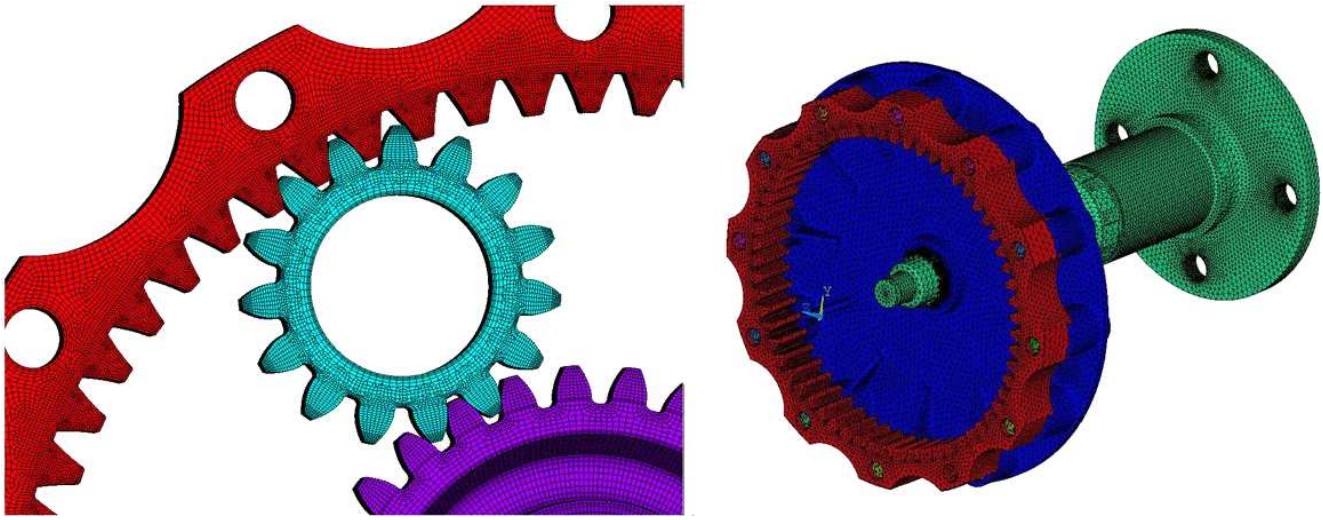

Fig. 2. A 3D model with FEM mesh: sun gear-satellite-coronary gear (on the left), the propeller shaft with ring gear (on the right)

The complete model of gear with propeller shaft and FEM mesh is shown in Fig. 3. Five satellites transmit power from the sun gear to the ring gear. Kinematics of propeller speed reduction unit at a certain ratio requires the yoke to be fixed.

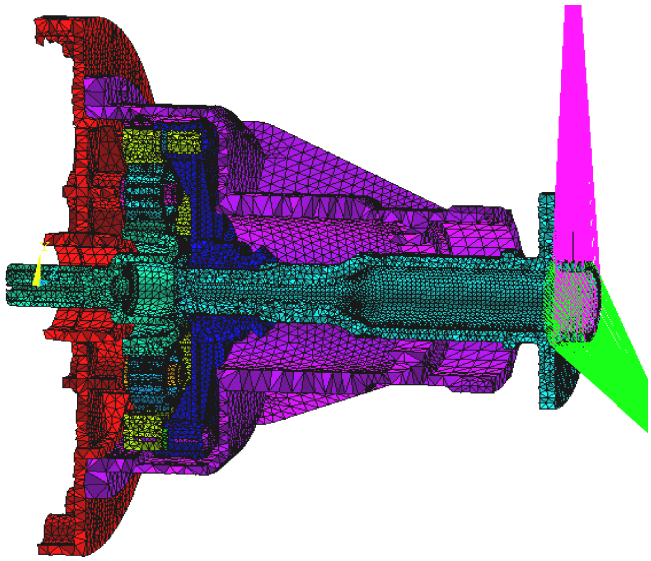

Fig. 3. Complete 3D model of gear with propeller shaft and FEM mesh

The model was made by dividing the propeller structure into elements of type SOLID 186 with intermediate nodes [622980 nodes] (Fig. 4). The propeller was modeled with mass elements – MASS21. The importance of selecting the right type of elements is shown below. There is a comparison of a twisted model of shaft with the gear model designed using different finite element types Commonly, detailed mesh parameters and discretization errors are omitted by authors [3].

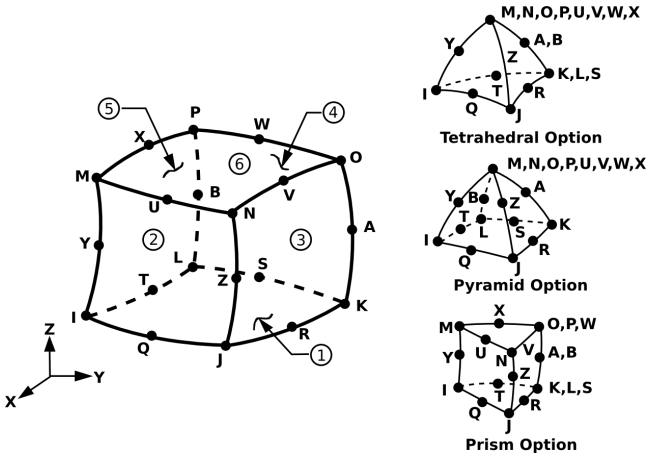

Fig. 4. FEM elements used

To illustrate the difference in mapping the stiffness of a structure in a correct manner using different element types a modal analysis of a cantilever beam was performed. The first two frequencies and mode shapes were computed. We took the solution of quadratic hexahedra elements as a reference solution and compared the results with a mesh of quadratic tetrahedra and linear tetrahedra having a coarse mesh and a fine mesh respectively. The results are shown in Table 1 [4, 5].

Table 1
Differences in the computed natural frequencies depended on the type of used finite elements

Frequency mode	Hexahedra quadratic [Hz]	Tetrahedra quadratic [Hz]	Tetrahedra linear coarse Hz	Tetrahedra linear fine Hz
1	0.5763	0.5712	8.461	1.132
2	3.735	3.705	52.306	7.047

Table 1 shows the differences in the computed natural frequencies, which depends on the finite elements used in the simulations of vibrations of the shaft.

Figure 5 shows a 3D model of the propeller shaft modeled with linear tetrahedral and hexahedral FEM elements. Figure 6 shows the results of the angle of twist of FEM simulations for this model. Figure 7 shows the results of measuring the twist angle as a function of the torque on the bench.

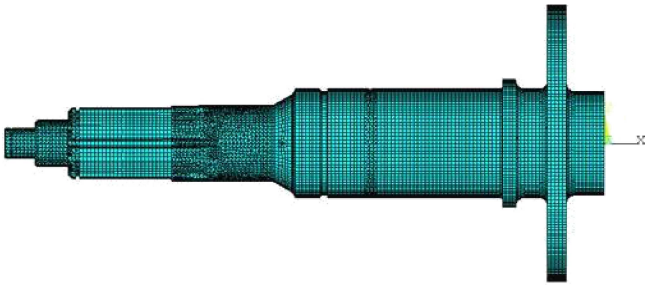

Fig. 5. Propeller shaft modeled with tetrahedron linear and hexahedra FEM elements

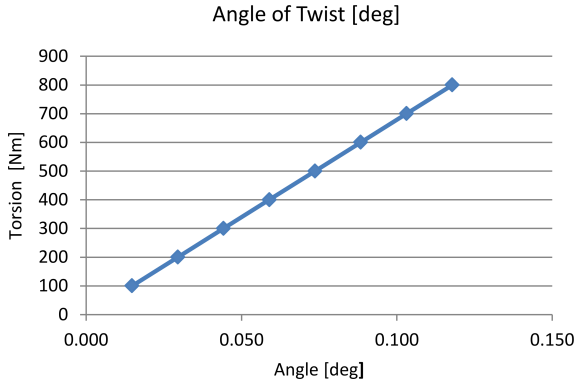

Fig. 6. Angle of twist of the propeller shaft modeled with tetrahedron linear and hexahedra FEM elements

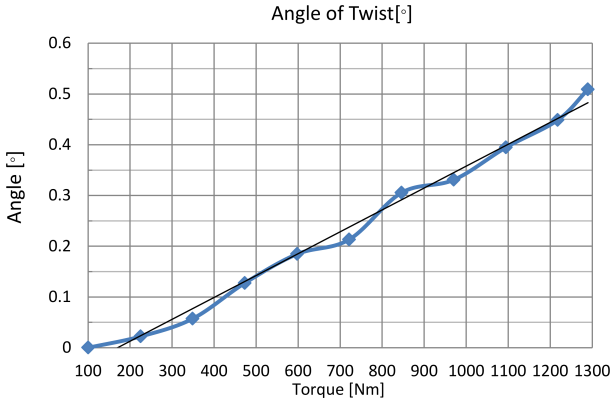

Fig. 7. Angle of twist of the propeller shaft measured on the bench

As it is seen the FEM simulation of a modeled shaft has about two times higher angle of twist that was measured on the bench. In complex structures, these differences in measurement and simulation are smaller than in simulation of simple objects like shafts and beams. The results obtained for the unloaded propeller speed reduction unit in the functions of FEM elements are given in Table 2.

The use of a linear type tetrahedron elements reduces the simulation time but it gives a significant problem both in analysis and in calculating modal stresses [5, 6].

Table 2
Differences in angle of twist depended on the type of used finite elements

Vibration mode	UNLOADED STATE (no rotation, no torque)		
	Gear version – axle diameter 40 mm, removed bearing from the end of propeller shaft, modified casing, Tetrahedral linear elements	Gear version – axle diameter 40 mm, removed bearing from the end of propeller shaft, modified casing, SOLID186 elements with intermediate nodes	Change in frequency caused by the introduction of elements of intermediate nodes
	[Hz]	[Hz]	[%]
1	45.9	38.4	−16
2	45.9	38.4	−16
3	50.0	46.9	−6
4	90.7	90.2	−1
5	115.5	101.6	−12
6	115.6	101.7	−12
7	335.6	323.5	−4
8	335.6	323.6	−4
9	878.6	664.2	−24
10	1172.4	898.3	−23
11	1235.3	928.0	−25
12	1504.3	1078.7	−28
13	1590.6	1122.7	−29
14	1602.6	1217.8	−24
15	1875.7	1416.6	−24

3. Simulation of natural vibrations of planetary gear unit 3D model

Simulations of vibrations were carried out for the unloaded and loaded gear with "takeoff power" torque and inertia forces. These simulations takes into consideration all material properties of steel and plastic damper elements. The 3D model assumed ideal geometry. The model No. 1 was analyzed with the casing with the casing full of symmetrical fins (Table 3). Then the model No. 2 was analyzed without two ribs and with a base for the propeller governor (Fig. 1). In the model No. 3, the diameter of the shaft was increased from 38 mm to 40 mm. In the modification of model No. 4, the bearing shaft was changed. The modal simulation results are shown in Table 4; visualizations of the selected modes are presented in Figs. 15–19.

Table 3
Natural frequencies – Model No 1

Mode of vibration	Unloaded	Loaded	Difference
	f [Hz]	f [Hz]	f [Hz
1	39.4	51.4	11.9
2	69.2	75.1	5.90
3	77.5	79.8	2.25
4	140.97	143.65	2.68
5	328.24	339.95	11.7
6	328.59	339.97	11.3
7	1036.9	1064.2	27.3
8	1055.5	1125.0	69.4
9	1185.6	1185.8	0.22
10	1206.0	1207.0	0.93

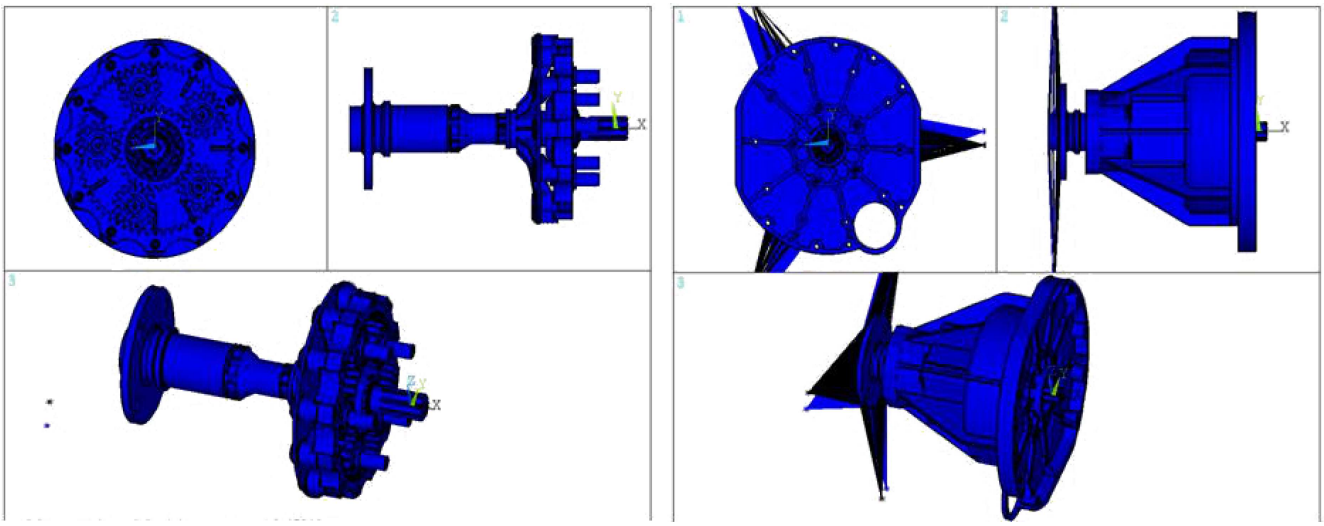

Fig. 8. First mode of vibrations – Model no 1, unloaded conditions

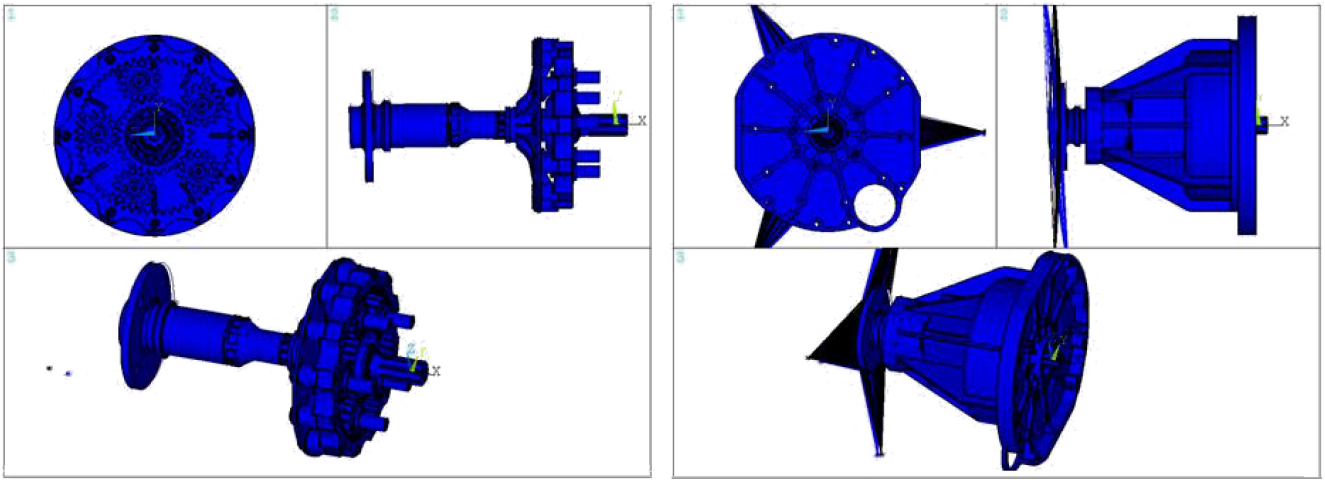

Fig. 9. Second mode of vibrations – Model no 1, unloaded conditions

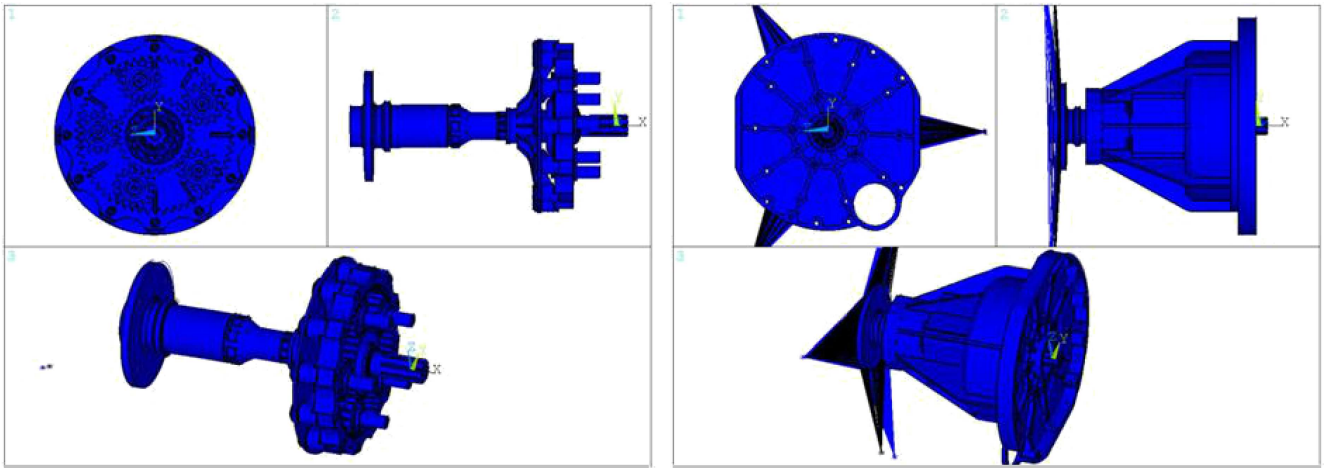

Fig. 10. Visualization of the third mode of vibrations – Model no 1, unloaded conditions

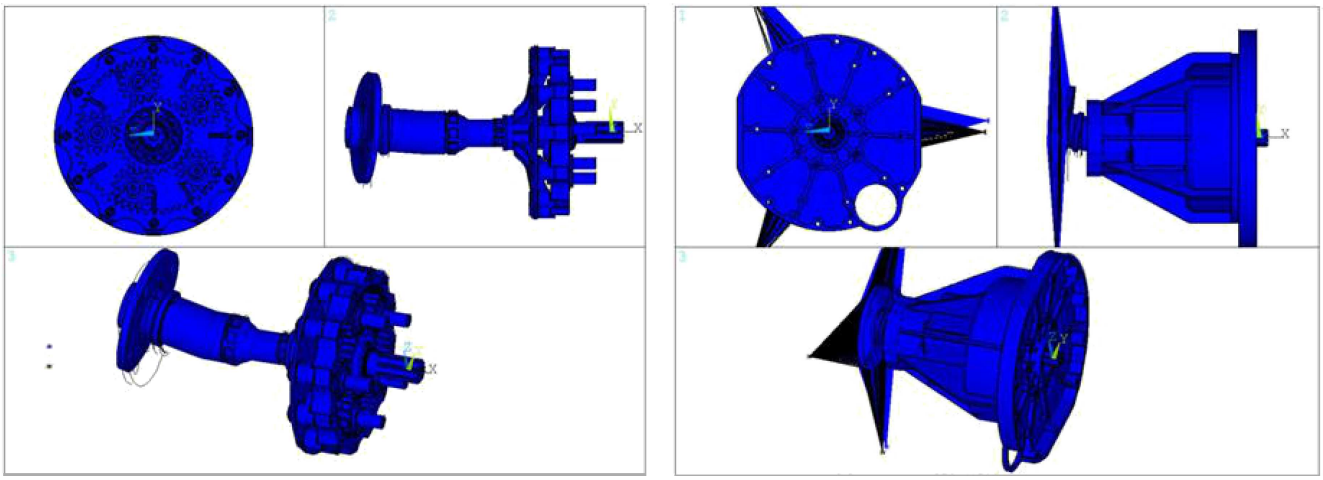

Fig. 11. Fifth mode of vibrations – Model No. 1, unloaded conditions

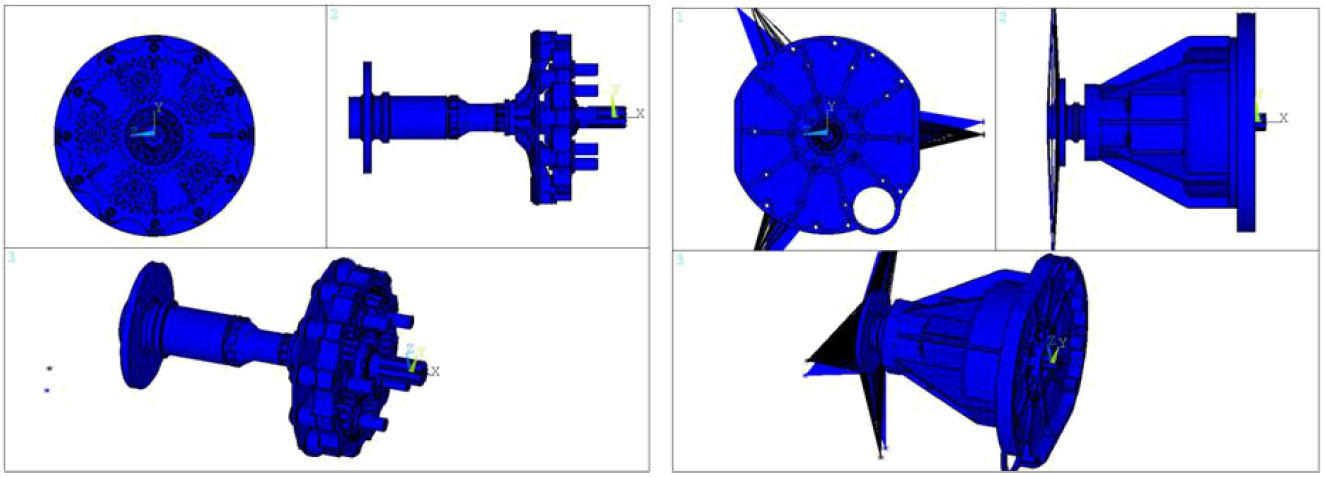

Fig. 12. First mode of vibrations – Model No. 1, loaded conditions

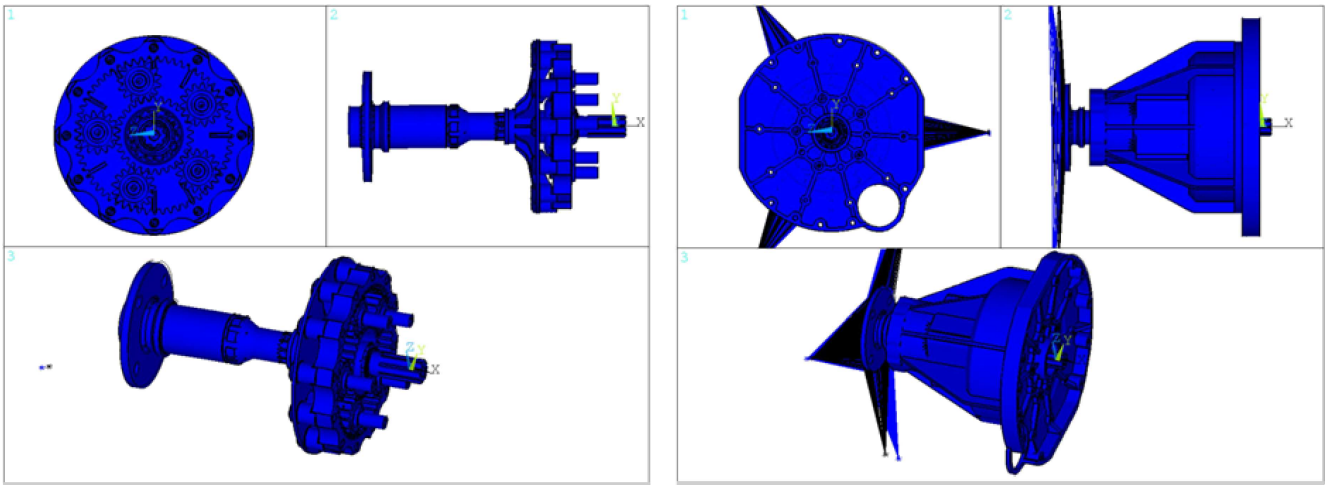

Fig. 13. Second mode of vibrations – Model No. 1, loaded conditions

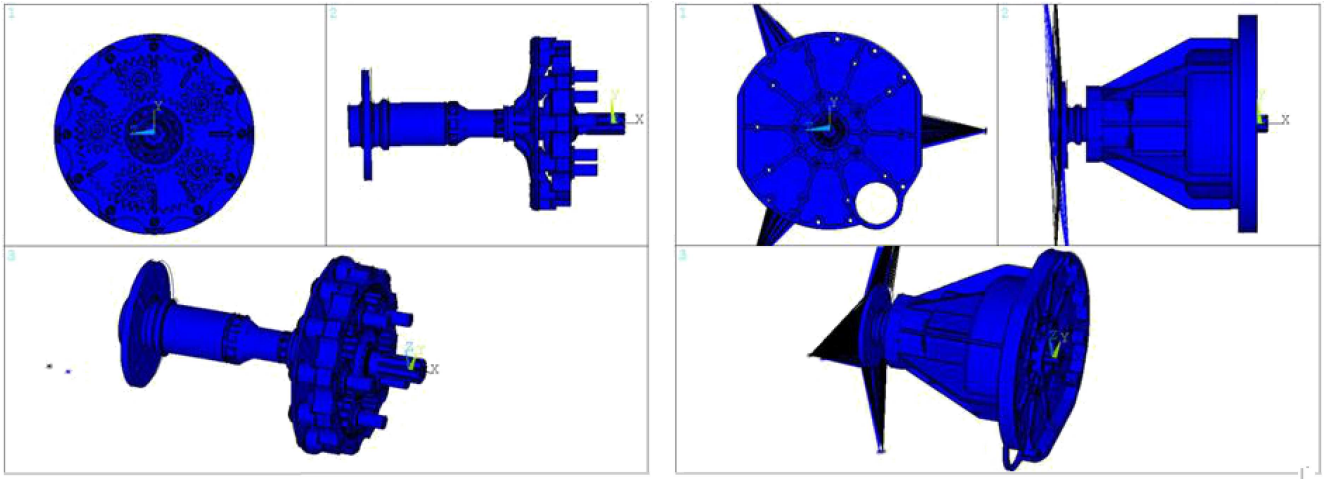

Fig. 14. Third mode of vibrations – Model No. 1, loaded conditions

Table 4
Natural vibrations – models No. 2, 3 and 4

Mode of vibration	Unloaded state (no rotation, no torque)			Loaded state (rotation, torque, cure/displacement)		
	Removed two ribs, shaft diameter 38 mm	Removed two ribs, shaft diameter 40 mm	Removed two ribs, shaft diameter 40 mm, removed bearing from the end of propeller shaft	Removed two ribs, shaft diameter 38 mm	Removed two ribs, shaft diameter 40 mm	Removed two ribs, shaft diameter 40 mm, removed bearing from the end of propeller shaft
	[Hz]	[Hz]	[Hz]	5400 rpm, 360 Nm	5400 rpm, 360 Nm	5400 rpm, 360 Nm
				[Hz]	[Hz]	[Hz]
1	39.3	47.15	38.4	60.2	52.55	47.6
2	40.2	51.48	38.4	60.3	52.58	47.6
3	45.2	50.47	46.9	68.5	56.73	56.3
4	82.0	128.7	90.2	93.5	123.3	90.3
5	112.7	131.1	101.6	119.9	137.2	107.9
6	113.1	131.47	101.7	120.2	137.55	107.9
7	674.3	664.22	323.5	694.2	810.76	327.6
8	750.3	808.86	323.6	755.0	814.84	327.7
9	756.1	812.95	664.2	760.7	682.68	683.9
10	923.8	906.67	898.3	983.8	965.55	958.0

Figures 8–10 show visualizations of the first three modes of vibration of unloaded model No. 1. Figures 12–14 show the first three forms of vibrations of loaded model No. 1, with load $M = 360$ Nm and inertia forces for $n = 5400$ rpm. A noticeable increase in the frequency of vibration of the first and the fifth to eighth modes are noticeable for load state seen in Table 3. Those are torsional and bending vibrations. Bending vibrations and torsional-bending of the propeller shaft are noticeable beginning with the fifth mode (Fig. 11).

In the loaded and unloaded conditions vibrations modes first, second and fifth to eighth are torsional and bent. The third mode represents torsional vibrations,, and forth torsional with axis symmetrical deflection (Fig. 15–18). It is interesting to note the ninth mode of vibration is pure axial vibration and the tenth is deflection without any twisting angle (Fig. 19). For all three models, an increase in the first three natural frequencies under operating load is shown. This frequency increase is not evenly distributed over models. For model No. 2, it is the highest, about 50% higher for first three modes of vibrations. For model No. 3, an increase of 9 to 12% was obtained. For model No. 4, growth within 20–40% was observed. For higher mode of vibrations, the differences are very small and only the 10th mode shows a 5% to 6% increase in frequency.

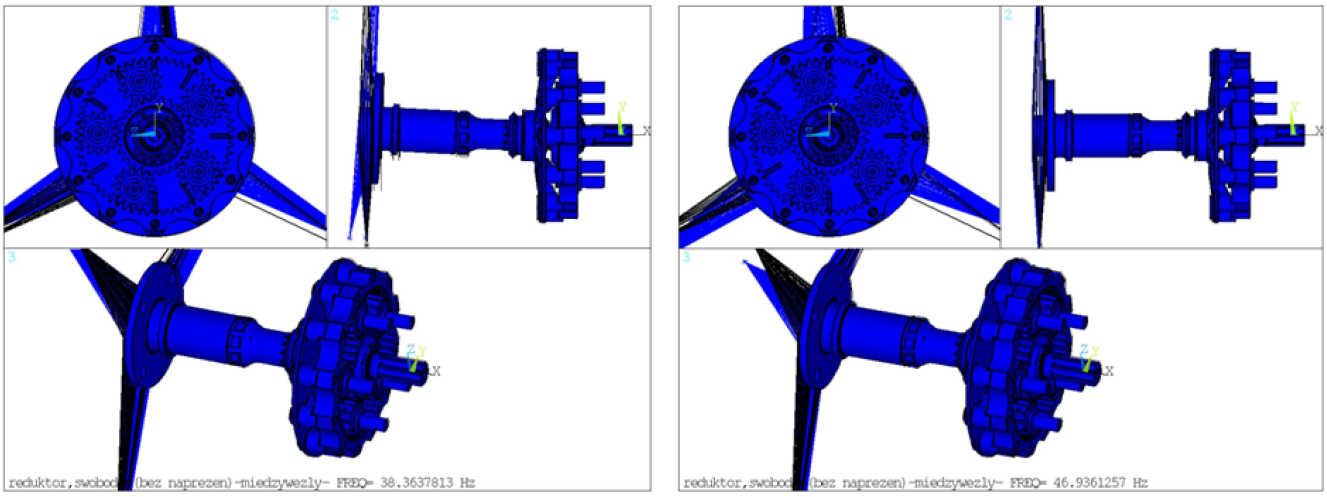

Fig. 15. First and third modes of vibrations – Model no 4, unloaded conditions

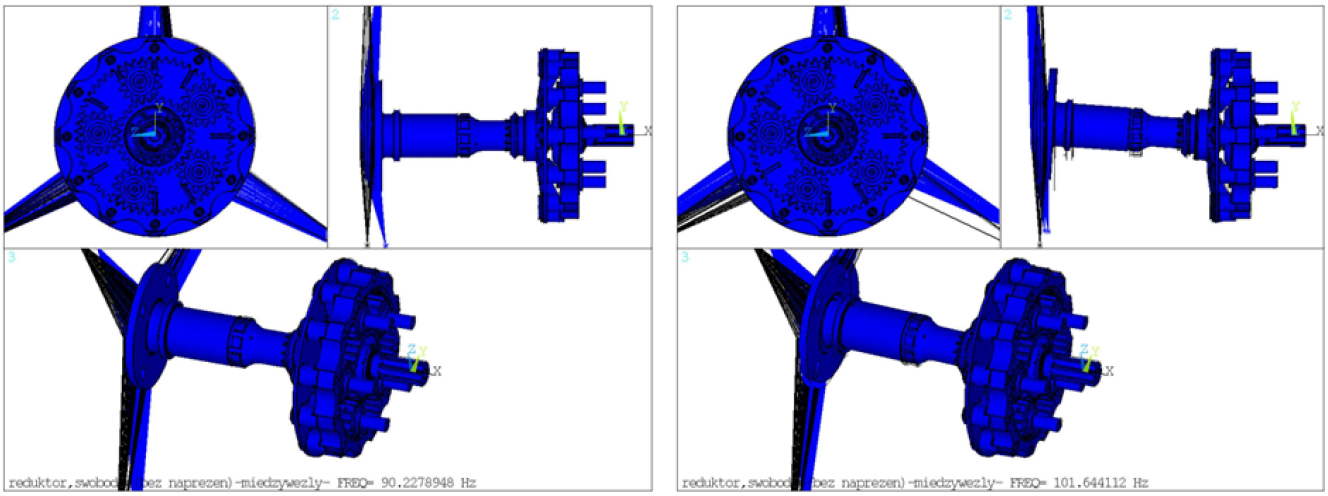

Fig. 16. Fourth and fifth modes of vibrations – Model No. 4, unloaded conditions

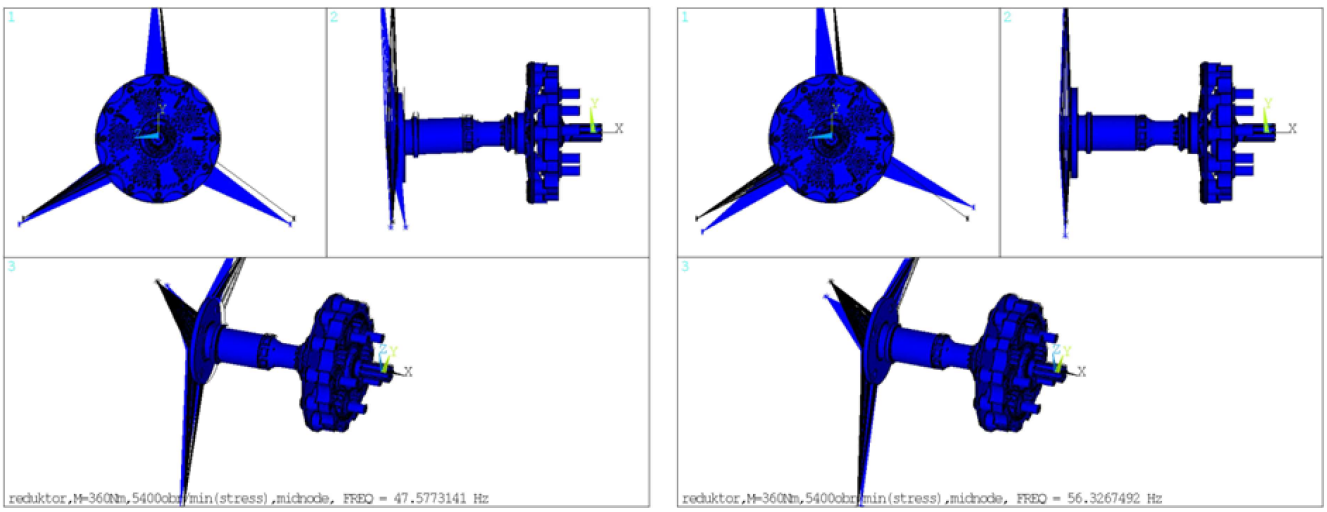

Fig. 17. First and third modes of vibrations – Model No. 4, loaded conditions

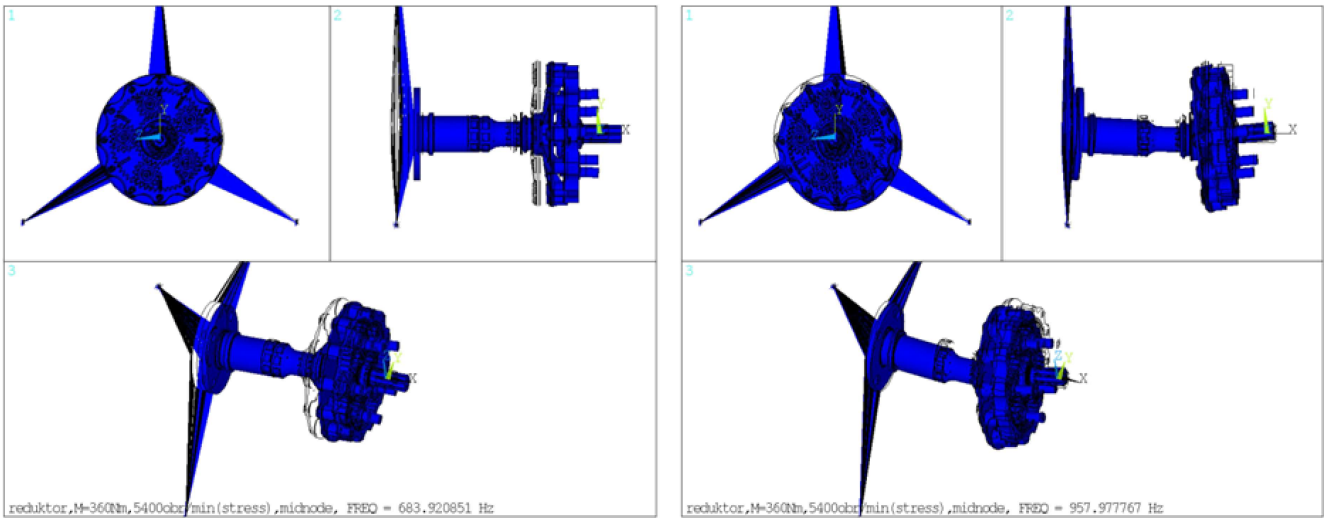

Fig. 18. Fourth and fifth modes of vibrations – Model No. 4, loaded conditions

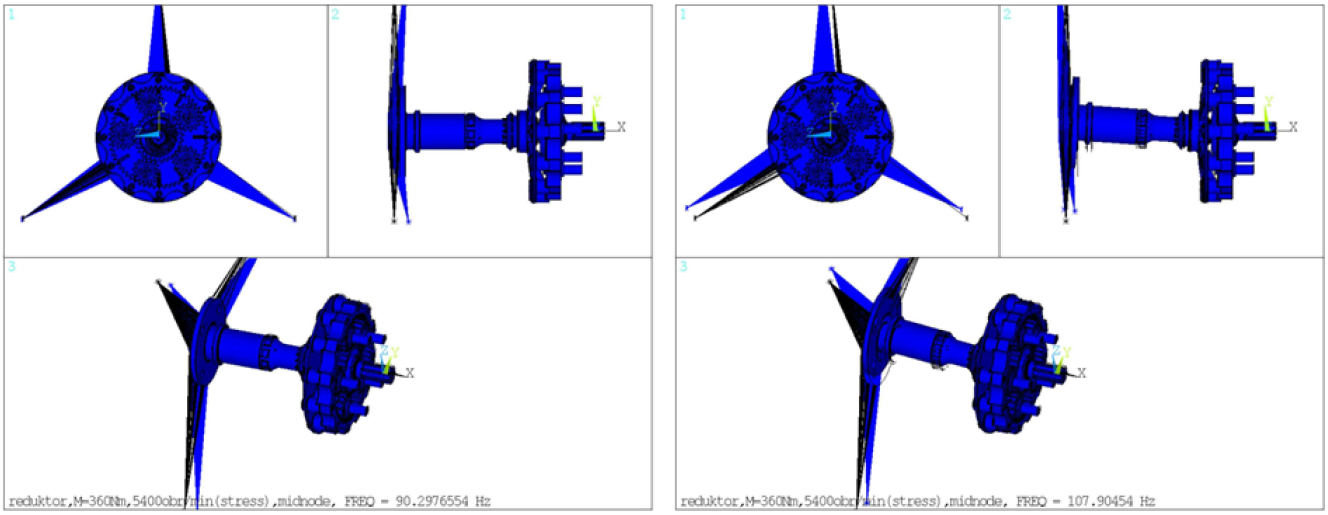

Fig. 19. Ninth and Tenth modes of vibrations – Model No. 4, loaded conditions

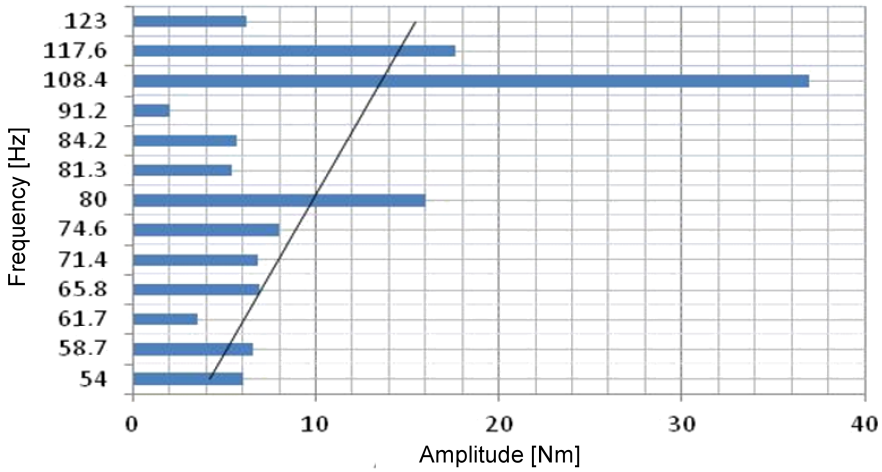

Fig. 20. Aircraft engine vibration amplitudes $N = 200$ kW with propeller speed reduction unit – bench test

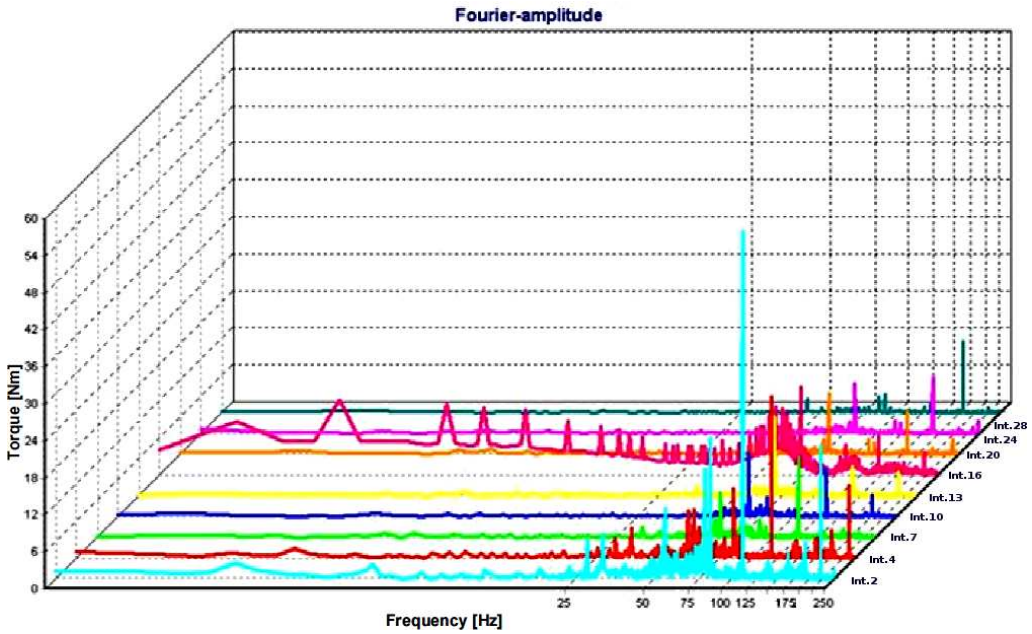

Fig. 21. Amplitudes of the propeller shaft torsional vibrations of aircraft engine $N = 200$ kW – summary graph

Figure 19 shows the amplitudes of harmonic vibrations selected from the common graph shown in Fig. 20 – test bench of engine vibrations [1]. Higher harmonics are skipped due to the low amplitude values. Finally, the design of the propeller speed reduction unit was based on model No. 3. While analyzing the results from Table 4 and Fig. 19 and 20, in some cases propeller speed reduction unit vibration frequencies and torsional vibrations frequencies were found to be overlapping. In the case of the analysis of model No. 4 under loaded conditions, the closeness of frequency 107.9 Hz to the frequency 108.4 Hz at the highest amplitude may cause dangerous conditions. Amplitudes for very similar frequencies of the speed reduction unit and engine model in the range of 54–61.7 Hz and 123 Hz are not significant. Proper distribution of vibrations in model No. 1 was observed with the exception of the third mode of vibrations ($f = 79.9$ Hz) that is identical to the third in the amplitude value in Fig. 19. In practice, the casing should be changed to model No. 2 or higher due to the possibility of propeller governor mounting.

4. Bench testing of the propeller speed reduction unit before and after the engine bench tests

The prototype gearing was tested on a laboratory stand in order to assess the gearing's quality and technical condition (Fig. 22). Tests were carried out without external load with the rotational speed $n <= 4800$ rpm [2]. Before engine bench test were conducted some measurements with external oil pump for gear lubrication were done. Shaft torsional vibration signals transmitted from a rotating propeller shaft were measured using radio communication equipment (ESA Messtechnik GmbH). Vibrations of the speed reduction unit after engine bench tests were conducted with splash lubrication. Measurements for various rpm's were repeated for different levels of oil. Following the engine bench test, measurements of gearing unit stiffness characteristics were also performed.

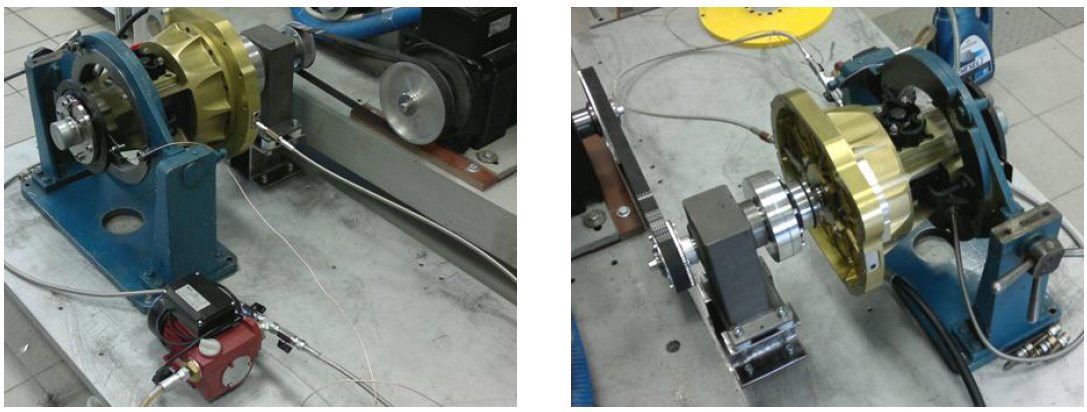

Fig. 22. Measurement of vibrations of a speed reduction unit mounted on a laboratory stand

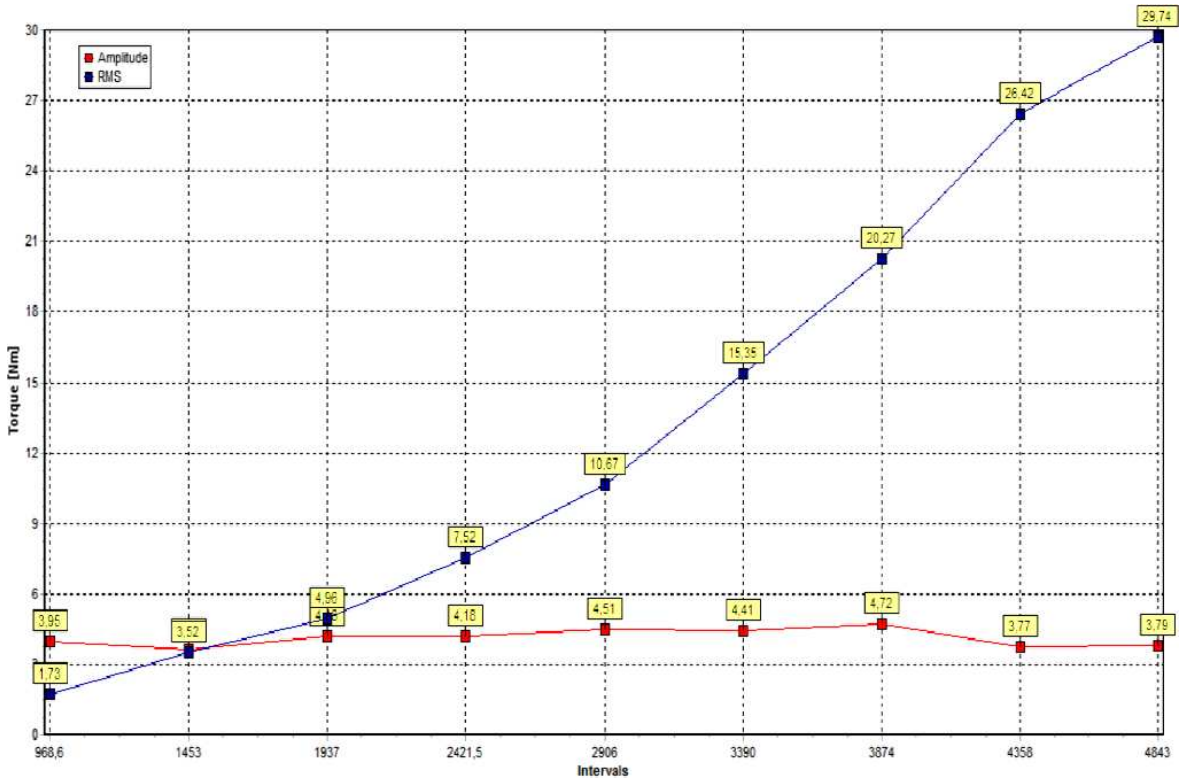

Fig. 23. Average torque RMS and vibrations amplitude of propeller speed reduction unit for unloaded conditions before engine bench test as a function of rpm. Propeller speed reduction unit with pressure lubrication

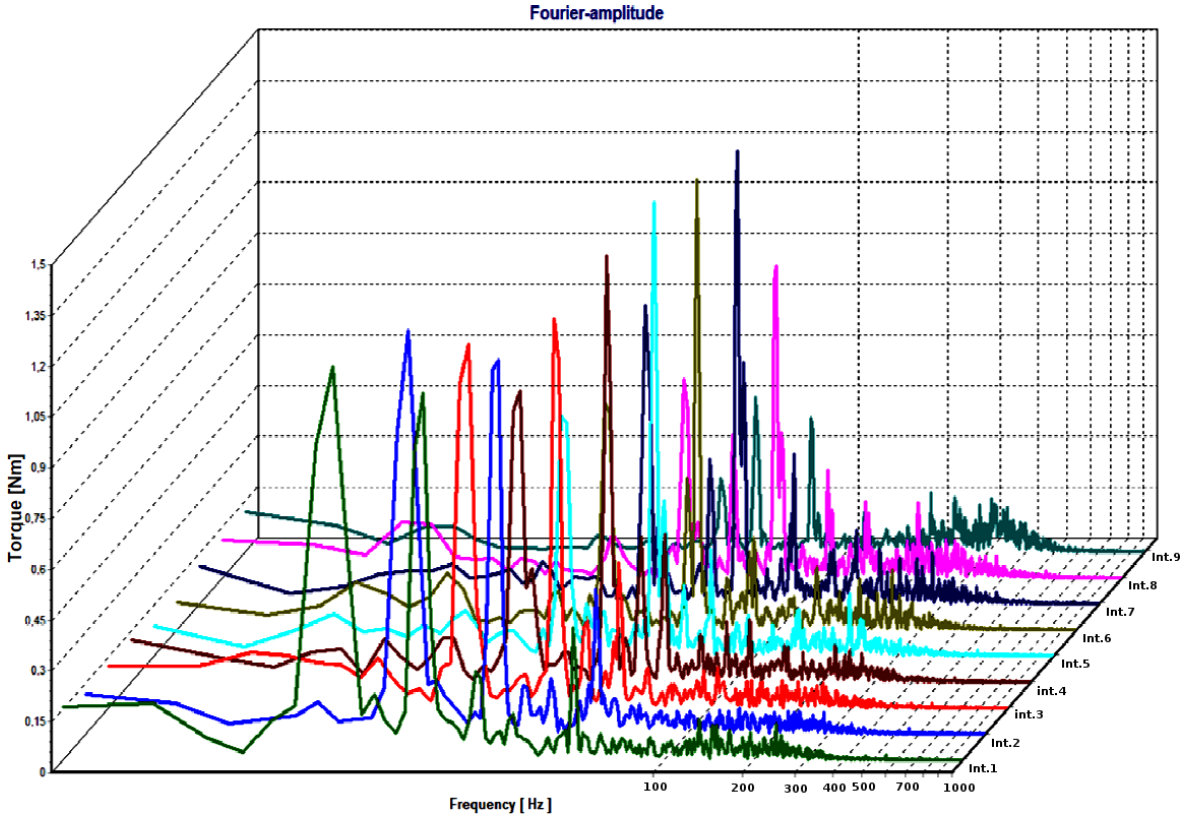

Fig. 24. Cumulative torsional vibrations of propeller speed reduction unit for unloaded conditions. Amplitudes as a function of rotational speed. Rotational speed range 980–4400 rpm corresponds with Charts 1–8. Before engine bench test

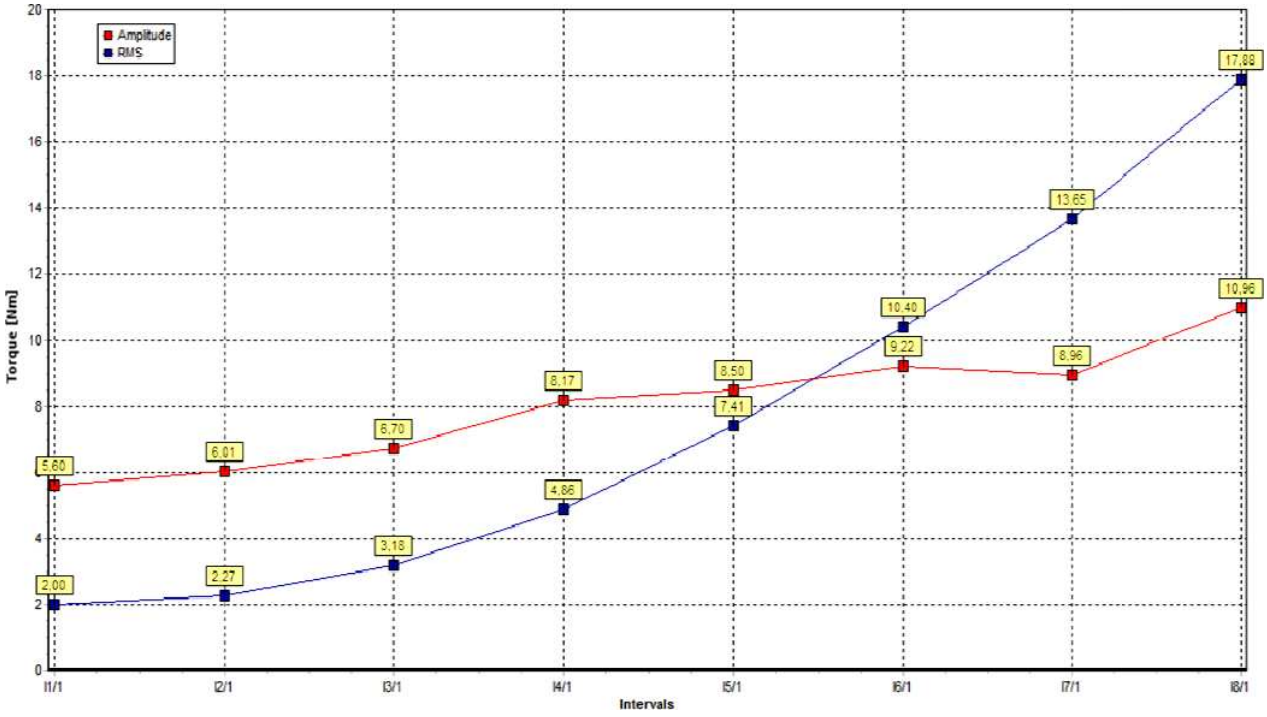

Fig. 25. Average torque RMS and vibration amplitude of propeller speed reduction unit in unloaded state after engine bench test as a function of rpm. Propeller speed reduction unit was splash lubricated. Low level of oil

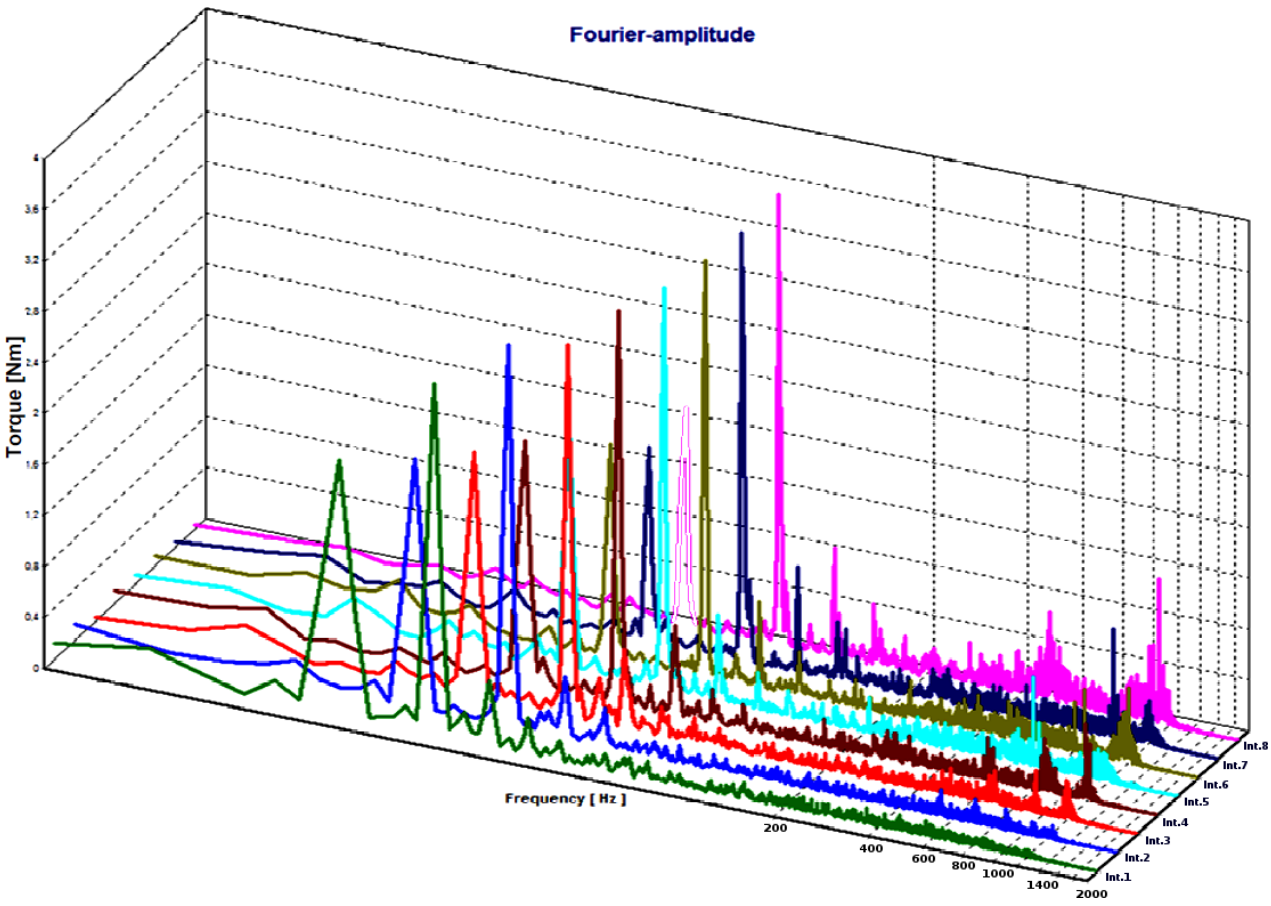

Fig. 26. Cumulative torsional vibrations of propeller speed reduction unit for unloaded conditions. Amplitudes as a function of rpm. Rotational speed range 980–4400 rpm corresponds with Charts 1–8. After engine bench test

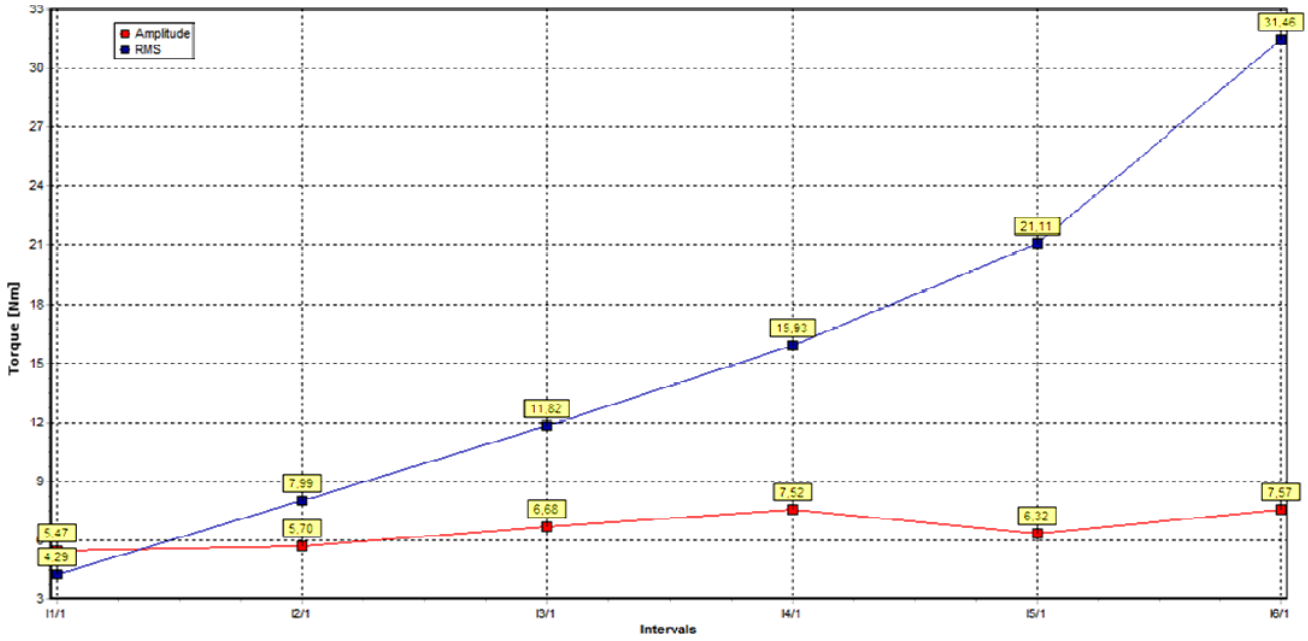

Fig. 27. Average torque RMS and vibrations amplitude of propeller speed reduction unit for unloaded conditions after engine bench test as a function of rotational speed. Propeller

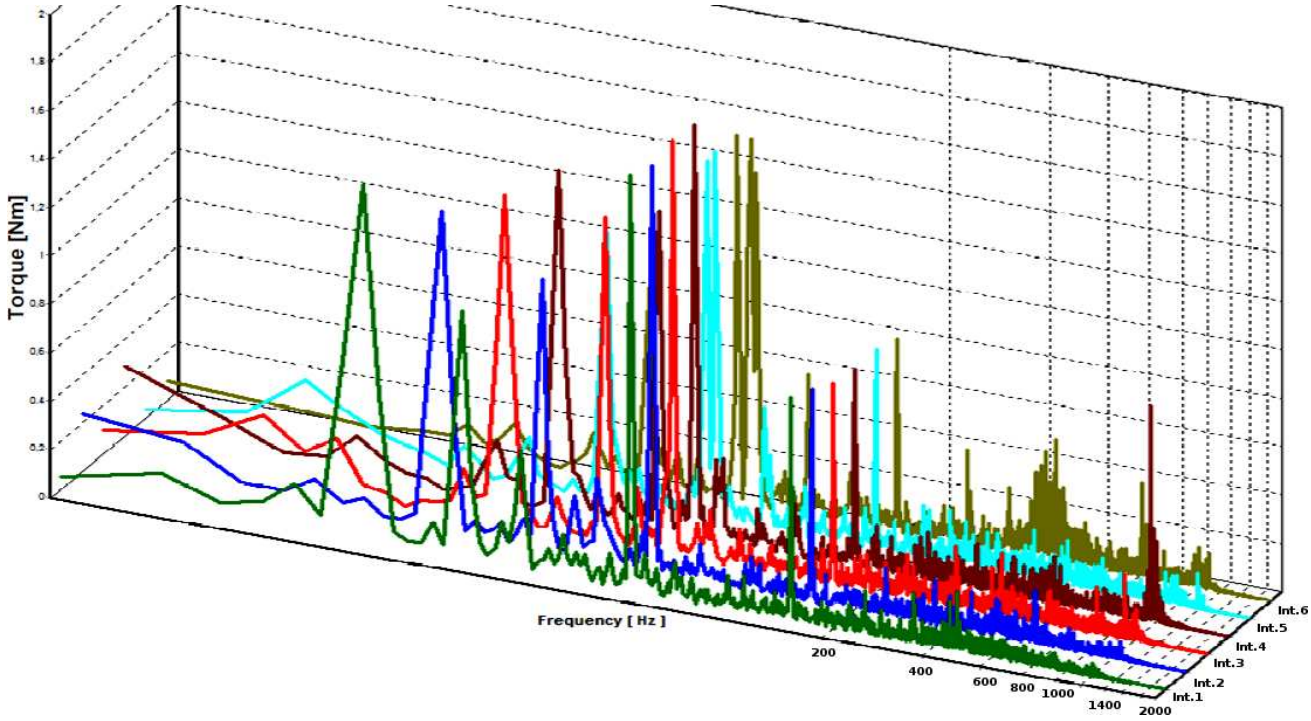

Fig. 28. Cumulative torsional vibrations of propeller speed reduction unit for unloaded conditions. Amplitudes as a function of rpm. Rotational speed range 980–3800 rpm corresponds with Charts 1–7. After engine bench test

The measurements after the engine bench test were carried out without an oil pump, with a low level of transmission oil [2]. There was no oil pressure, and no oil was sprayed on the gears. The result is lower torque (Fig. 25) compared to the results with pressure lubrication (Fig. 23). Amplitudes of the first and half of vibrations harmonic frequencies are, respectively, from 1.5 to 2.5 times higher than before the engine bench test. Radial run out of propeller shaft after engine bench test did not exceed 0.02 mm.

Increasing the oil level to the maximum level resulted in increasing torque significantly. The oil temperature quickly rose to 80°C. Resistive torque Mop = 31 Nm has been

achieved at a speed of $n = 3400$ rpm. Resistive torque of Mop = 29.74 Nm at $n = 4800$ rpm and oil temperature of 45°C was obtained with spray lubrication. The level of vibration induced internally (manufacture and assembly errors) recorded before engine bench test was satisfactory. The maximum amplitude of vibration was within 11% of the value of resistive torque at $n = 4800$ rpm. After the engine bench test, damping elements were stiffened. A minimum clearance at the elastic elements of satellite gears rear bolts was created. The plastic sleeves at the junction of the ring gear and the propeller drive shaft were strengthened. This resulted in decreasing the elastic deformation of damping elements. This also resulted in increasing the propeller speed reduction unit vibration amplitudes. During gear failure investigations some modern neural network techniques can be used [7]. The results of the propeller shaft and complete propeller speed reduction unit torsional stiffness measurements are shown in Figs. 7 and 29.

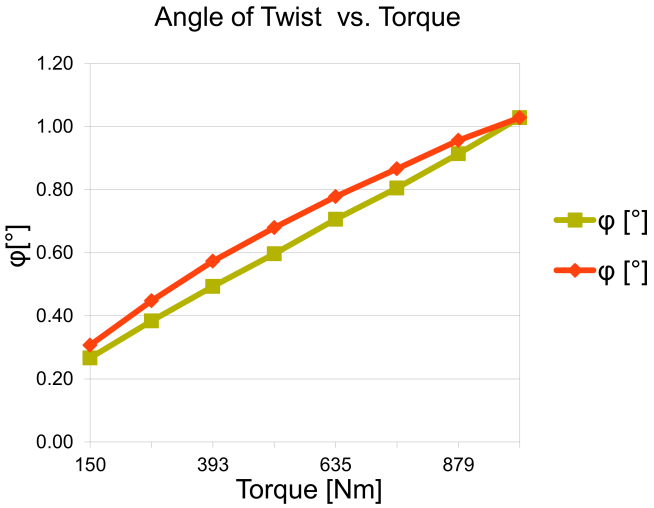

Fig. 29. Elastic torsional half-characteristics of the propeller speed reduction unit

The torsional stiffness of the propeller shaft was: $Kw = 7270$ Nm/deg, while torsional stiffness of propeller speed reduction unit with elastic silencers was: $Cr = 1000$ Nm/deg.

5. Conclusions

Simulations of the vibration propeller speed reduction unit prototype developed for 3D model with modifications facilitated:

- identification of vibration in the spectrum of vibration engine drive,
- choice of the design variant of propeller speed reduction unit.

The examples from Sec. 2 showed that different element types had a significant impact on the simulation results. We do not recommend using linear-type tetrahedron elements due to over estimated simulation results significant positive simulation error with respect to the exact solution.

The measurement of vibrations in reducing gear that was not loaded, before and after testing on bench, made the following possible:

- evaluation of intermediate precision manufacturing and gear mounting,
- evaluation of the impact of the type of lubrication and oil level on the resistive torque,
- evaluation of the impact of the type of lubrication and oil level on the amplitude of vibrations (main and half-harmonic),
- authoritative assessment of the state of the propeller speed reduction unit

The elastic elements were significantly worn. The material that had parameters similar to that of clutch inserts was permanently deformed. Stiffness increased and grip decreased to zero. It strongly influenced the increasing of vibration amplitude. Metrological tests and an verification the disassembled propeller speed reduction unit parts confirmed the good condition of the gears and bearings. Elastic elements were to be replaced. The choice of more reliable elastic material for sleeve satellites and ring gear bolts is strongly recommended.

REFERENCES

[1] W. Ostapski, "New generation, high output (200 kW), multi-fuel, environmental friendly, aircraft reciprocating engine, design and development", *Development Project Report* Number 6ZR62008C/07057 (2008), (in Polish).

[2] W. Ostapski, *Propeller Engine Test Bench Project for WSK-PZL-Kalisz S.A.*, (Nr 1/TR/WSK/2011), Kalisz, 2011, (in Polish).

[3] L. Kwaśniewski, "Application of grid convergence index in FE computation", *Bull. Pol. Ac.: Tech.* 61 (1), 123–128 (2013).

[4] E. Wang, T. Nelson, and R. Rauch, "Back to elements – tetrahedra vs. hexahedra", *CAD-FEM GmbH, ANSYS Conf.* 1, 1–16 (2004).

[5] ANSYS Theory Reference, Release 6.1, *Swanson Analysis Systems*, Inc., (2001).

[6] S.E. Benzley, E. Perry, K. Merkley, and B. Clark, "A comparison of all-hexahedra and all tetrahedral finite element meshes for elastic & elastoplatic analysis", *Proc. 4th Int. Meshing Round table Sandia National Labs* 1, 179–181 (1995).

[7] C.T. Kowalski and M. Kamiński, "Rotor fault detector of the converter – fed induction motor based on RBF neutral Network", *Bull. Pol. Ac.: Tech.* 62 (1), 69–76 (2014).